

# MEDIRL: Predicting the Visual Attention of Drivers via Maximum Entropy Deep Inverse Reinforcement Learning

Sonia Bae<sup>†</sup>, Erfan Pakdamanian<sup>‡</sup>, Inki Kim<sup>‡</sup>, Lu Feng<sup>†</sup>, Vicente Ordonez<sup>†</sup>, Laura Barnes<sup>†</sup>

<sup>†</sup> University of Virginia, <sup>‡</sup>University of Illinois at Urbana Champaign

<sup>†</sup>{sb5ce,ep2ca,vicente,lu.feng,lb3dp}@virginia.edu, <sup>‡</sup>inkikim@illinois.edu

## Abstract

Inspired by human visual attention, we introduce a Maximum Entropy Deep Inverse Reinforcement Learning (MEDIRL) framework for modeling the visual attention allocation of drivers in imminent rear-end collisions. MEDIRL is composed of visual, driving, and attention modules. Given a front-view driving video and corresponding eye fixations from humans, the visual and driving modules extract generic and driving-specific visual features, respectively. Finally, the attention module learns the intrinsic task-sensitive reward functions induced by eye fixation policies recorded from attentive drivers. MEDIRL uses the learned policies to predict visual attention allocation of drivers. We also introduce EyeCar, a new driver visual attention dataset during accident-prone situations. We conduct comprehensive experiments and show that MEDIRL outperforms previous state-of-the-art methods on the following large-scale driving attention benchmark datasets: DR(eye)VE, BDD-A, and DADA-2000. The code and dataset are provided for reproducibility.<sup>1</sup>

## 1. Introduction

Autonomous vehicles have witnessed significant advances in recent years. These vehicles promise better safety and freedom from the prolonged and monotonous task of driving. However, one of the remaining safety challenges of vision-based models integrated into these vehicles is how to quickly identify important visual cues and understand risks involved in traffic environments at a time of urgency [43]. Humans have an incredible ability to quickly detect the most relevant stimuli and direct attention to potential hazards in complex situations [54, 37, 36] through a combination of bottom-up (*stimuli driven*, e.g., color and intensity) and top-down (*task driven*, e.g., current goals and knowl-

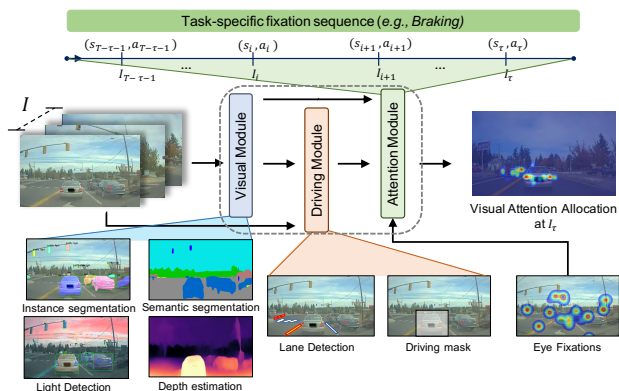


Figure 1: MEDIRL (Maximum Entropy Deep Inverse Reinforcement Learning). Given an input video and corresponding eye fixations, MEDIRL learns to model the visual attention allocation as a sequence of states and actions  $(s_t, a_t)$ . MEDIRL has a visual module that extracts general frame features, a driving module that extracts driving specific visual context features, and an attention module that learns policies for modeling transitions in  $(s_t, a_t)$ .

edge) mechanisms [11, 21]. For instance, in the dynamic driving environment where top-down factors change from turning left to braking, the driver’s attention shifts from the car in the adjacent lane to the lead car. This process helps humans to overlook objects that are irrelevant to their decisions and reduce the unnecessary complexity of scene understanding [7]. Despite recent progress in computer vision models for autonomous systems [22, 52], they are still behind the foveal vision ability of humans [35, 50].

We propose a framework that combines bottom-up and top-down attention to compute salient regions relevant to a driving task. In contrast, saliency detection models in the driving domain mostly rely on human gaze information [43, 51, 39]. However, low level cues obtained from gaze behavior without higher level semantic context do not completely capture everything a driver should attend to in critical situations. For instance, drivers might get distracted by irrelevant objects such as roadside advertisements. Ad-

<sup>1</sup>Code and dataset are available in <https://github.com/soniabaee/MEDIRL-EyeCar>

ditionally, the peripheral vision of humans allow fixating on one object while attending to another [51]. Finally, drivers usually maintain their visual attention at the center of the driving scene as this is where the vehicle is headed to [16, 39]. On the other hand, some recent visual attention models do consider high-level cues such as relevant semantic categories obtained through semantic image segmentation and scene parsing [23, 22, 25] but miss integrating eye fixation information [38]. Our work considers both contextual information and eye fixations in accident-prone situations.

In this paper we present MEDIRL, Maximum Entropy Deep Inverse Reinforcement Learning, a modular framework that learns the intrinsic reward functions and policies used by attentive drivers during accident-prone collisions. We modeled the driver’s gaze behavior as a dynamic state-action transition. These transitions were learned and then used to predict visual attention allocation of drivers.

Inverse Reinforcement Learning (IRL) [1, 60] is a form of imitation learning that enables a learning agent to acquire skills from expert demonstrations [44]. For example, if an autonomous system tries to locate the salient region of a driving scene at critical moments, the desired visual behavior can be demonstrated by studying the attention allocations of an attentive driver who effectively detects brake lights. In this way, a learning agent can infer a reward function explaining the expert’s behavior and optimize its own behavior accordingly. MEDIRL is a generalized framework and can be adapted to model visual attention in a variety of contexts. It consists of three modules: visual, driving, and attention modules (see overview in Figure 1). The *visual module* leverages features such as traffic density, distance to other cars, and brake lights. The *driving module* extracts features that are relevant to specific driving tasks. The *attention module* integrates the outputs of the previous two modules and learns the internal reward functions and policies used by attentive driver; drivers who significantly detect task-related visual stimuli. These policies and rewards are used to predict the visual attention allocations of drivers in rear-end collisions.

We validate the effectiveness of MEDIRL on three datasets: DR(eye)VE [39], BDD-A [51], and DADA-2000 [14]. Experimental results indicate that MEDIRL effectively learns visual attention policies of attentive drivers and outperforms prior works. Additionally, we introduce *EyeCar*, a novel dataset of driving videos of vehicles involved in rear-end collisions paired with eye fixation data captured from human subjects. The main contributions of this work can be summarized as follows:

- MEDIRL, a novel modular framework that leverages both visual context cues and eye fixation information to learn the reward functions and (near-) optimal policies of attentive drivers for modeling visual attention.

- We introduce *EyeCar*, a new dataset including both videos of rear-end collisions and associated human visual attention.
- We establish the state-of-the-art in predicting the visual attention allocation of drivers in several benchmarks – and across several metrics.

## 2. Related Work

Prior research has studied the pattern of eye movements connected to the tasks an observer is performing [32, 2]. Some of these works rely on the direct ties between eye movement and the ongoing demands of a target task [54, 42, 41]. Furthermore, with increased access to large-scale annotated visual attention datasets and advanced data-driven machine learning techniques, the prediction of human visual saliency has received significant interest in computer vision [48, 46, 26, 59, 9, 33]. Previous studies have used bottom-up visual saliency and visual search strategies over static stimuli [13, 28, 18, 15], and video [59, 47, 32, 33, 56]. A few works have also proposed top-down attention models for explaining sequences of eye movements [41, 5, 3]. We are interested in detecting the salient regions of a scene with respect to driving tasks by *estimating where the driver is looking* and, *detecting task-related objects of interest in their field of view*. A few pioneering works have already been proposed in the context of driving [19, 50, 16]. These methods present innovative ways of modeling the bottom-up saliency or top-down visual attention [39, 50, 51, 14, 23, 38]. Our work builds on this body of knowledge and goes beyond by considering task-related visual attention allocation from human drivers and combining it with eye fixation data. The recent work of [38] incorporates both a bottom-up and top-down strategy to predict the focus of attention of drivers. Similarly, we leverage a combination of bottom-up and top-down attention mechanisms to extract bottom-up and top-down visual context features of accident-prone situations. Previous reinforcement learning (RL) models have thus far mainly relied on bottom-up saliency over static stimuli [29, 31, 57] and have widely employed unimodal features in their prediction [30].

Our primary goal is to recover the intrinsic task-sensitive reward function [58] induced by visual attention allocation policies recorded from drivers in a complex driving environment. Based on both the remarkable ability of the human visual system to filter and extract relevant information in a timely manner and the recent progress of reinforcement learning approaches, we propose using deep IRL [60, 49]. Similar to our work, [54] recently proposed using IRL for modeling visual attention. Our proposed MEDIRL framework adopts IRL for complex and dynamic driving environments by taking into account a variety of other high level

	DR(eye)Ve	BDD-A	DADA-2000	EyeCar
collision	✗	✗	✓	✓
POV	✗	✗	✗	✓
speed	✓	✗	✗	✓
GPS	✓	✓	✗	✓
# vehicles	1.0	4.4	2.1	4.6
# frames	555k	318k	658k	315k
# gaze	8	45	20	20

Table 1: Compared to prior datasets, EyeCar is the only dataset captured from a point-of-view (POV) perspective, involving collisions, and including metadata for both speed and GPS. EyeCar also has the largest average number of vehicles per scene, and gaze data for 20 participants.

cues.

Our work is also related to previous works that have proposed image-based visual attention datasets [54, 8, 52, 40, 34, 4, 28, 18, 15, 47, 32, 55]. In the context of driving, however, only a few large-scale, publicly available, real-world videos with annotated visual attention exist. DR(eye)VE [39] and BDD-A [51] are the most well-known large-scale annotated datasets in naturalistic and in-lab driving settings, respectively. Importantly, the recently-released annotated driving attention dataset with in-lab settings, DADA-2000 [14], is the only available dataset capturing scenes of collisions. This is because it is nearly impossible to collect enough driver attention data for collision or near-collision events. EyeCar further contributes to this area by having a more diverse array of driving events, beyond looking forward and lane-keeping. Unlike DADA-2000, EyeCar uses a point-of-view perspective from the car involved in the accident. Table 1 compares EyeCar with similar datasets (more details in Sec. 4).

### 3. The MEDIRL Framework

MEDIRL is composed of visual, driving, and attention modules (Figure 1). Given a front-view video paired with eye fixation data captured from human subjects, we first use the visual module to extract generic visual context features from the video using models, such as semantic segmentation, instance segmentation, brake-light detection, and depth estimation (Figure 2). Second, we use the driving module to extract driving-specific features, such as lane detection of the ego-vehicle and location tracking from the lead vehicle (Figure 3-left). Finally, the attention module learns the policies to model the driver gaze behavior that matches the corresponding input videos (Figure 3-right).

#### 3.1. Visual Module

The visual module extracts low and mid-level visual cues that are useful for a variety of visual attention tasks. We rely on pre-existing models for semantic and instance segmentation, as well as depth estimation. In addition, we propose an

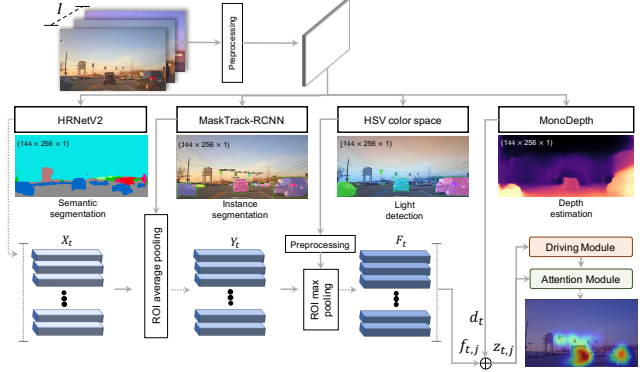


Figure 2: Overview of our *visual module* which extracts features using semantic segmentation, instance segmentation, light detection, and depth estimation. [Best viewed in color]

approach to detect brake lights and traffic lights. Figure 2 displays an overview of these individual components.

Given a set of driving video’s frames,  $I = \{I_t\}_{t=1}^T$ , we resize each of them to  $144 \times 256 \times 3$ , where  $T$  is the number of frames. Then we normalize each frame by subtracting the global mean from the raw pixels and dividing by the global standard deviation.

**Semantic and Instance Segmentation:** We use HRNetV2 [45] that is pre-trained on Mapillary Vistas street-view scene dataset [34] as the backbone net to extract pixel-wise category prediction along with the object bounding boxes in a frame. Therefore, we obtain a high-level visual representation of a given frame at each time step  $t$ . It should be noted that we have a single frame in each time step. This representation  $X_t$  contains a set of 256-dimensional latent vectors over the spatial dimension,  $X_t = \{x_{t,1}, \dots, x_{t,l}\}$ , where  $l = w \times h$  is the spatial dimension ( $w$  and  $h$  denote width and height of a frame, respectively). To further provide object-related visual attention, highlighting more precise salient regions, we use an instance detection model, MaskTrack-RCNN [53]. This model predicts instance masks as well as their locations and categories during a video. To obtain the visual feature representations of the extracted regions  $Y_t$ , we aggregate each predicted interest region of interest (ROI) to the latent vectors  $x_{t,j}$ , for  $j = \{1, 2, \dots, l\}$  by using a position-sensitive ROI average pooling layer.

**Light Detection:** Any rear-end collision includes salient stimuli such as brake lights. To detect this type of stimuli, we convert each frame to HSV color space. First, we calculate the average brightness level of each vehicle and traffic light masks (extracted from MaskTrack-RCNN) over  $I$ . Then, we calculate the brightness anomaly of the selected masks by subtracting their average brightness value from their actual brightness level at each time step  $t$ . Therefore, we can determine the pixels corresponding to these anomalies as well as their time of occurrence. As both low

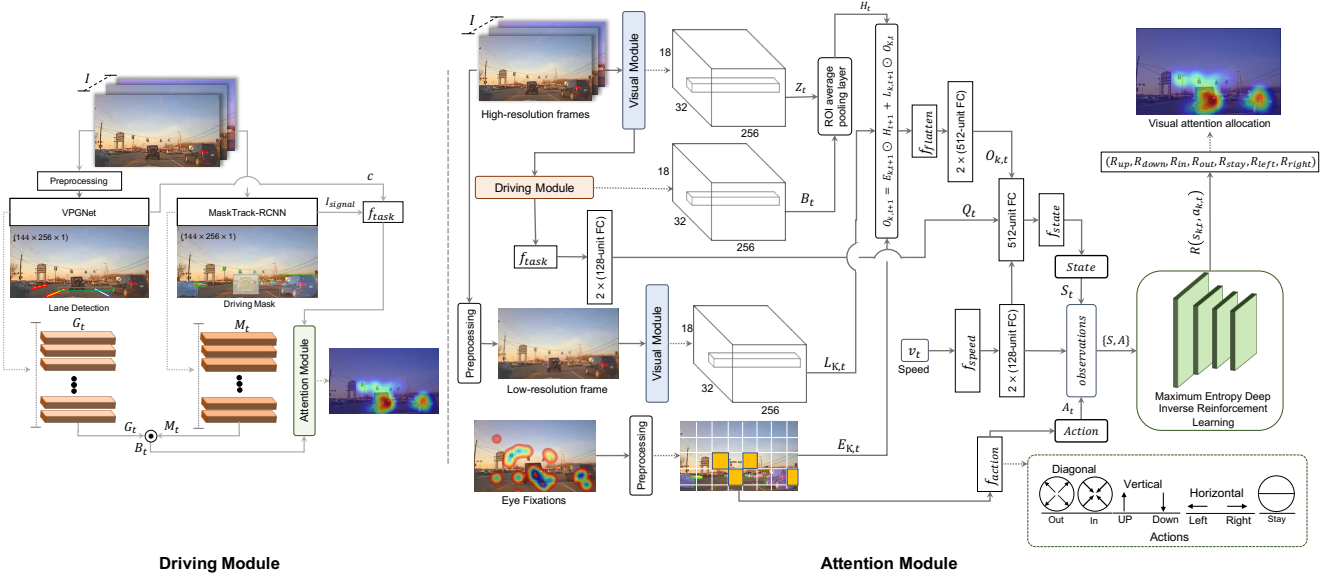


Figure 3: **Left:** Overview of our *driving module* which extracts driving specific visual context features as well as the types of driving tasks in rear-end collisions. **Right:** Overview of our *attention module* which takes the driving specific visual context information, the eye fixation, and the current speed of the ego-vehicle as an input. Our model provides the reward for the next action based on the learned policy of attentive drivers visual attention allocation. [Best viewed in color]

and high-level visual cues are important, we concatenate the predicted lights’ locations to the feature vector  $Y_t$ . We use a position-sensitive ROI max pooling layer to aggregate the latent vectors  $y_{t,j}, j = \{1, 2, \dots, l\}$  for each light location to obtain the visual feature  $F_t$ . Thus,  $F_t$  contains a set of 256-dimensional latent vectors over the spatial dimension.

**Depth Estimation:** Recognizing the relative distance to the other traffic participants (e.g., the lead vehicle) is crucial for making optimal driving decisions. Therefore, we use a supervised monocular depth estimation model, Monodepth2 [17], to amplify nearby regions (e.g., distance to a target object) of a driving scene. The predicted dense depth map  $D_t$  at each time step  $t$  is combined with the visual feature  $F_t$  by following formula:  $Z_t = F_t \oplus D_t$  where  $F_t \oplus D_t = F_t \odot \lambda * D_t + F_t$ , and  $\lambda = 1.2$  is an amplification factor.

### 3.2. Driving Module

The driving module extracts driving-specific visual features for driving tasks. Overview of the driving module is shown in Figure 3.

**Lane Changes:** The lane marking detection is critical for a task-related visual attention allocation of drivers, as an indicator of the type of maneuver. Instead of training a ConvNet from scratch, we use a pre-trained lane detection model, VGPNet [27]. The VGPNet model is a unified end-to-end trainable multi-task network that jointly handles lane and road marking detection. Therefore, we can recognize left and right lanes of the ego-vehicle by delineating

their boundaries. We capture a high-level driving specific contextual representation  $G_t$  of a given frame at each time step  $t$  including a set of latent vectors over the spatial dimension  $l$ .

**Driving Mask:** To emphasize the importance of the lead vehicle in rear-end collisions, we use MaskTrack-RCNN [53]. To recognize the lead vehicle, we select the biggest bounding box which encapsulates all the pixels of the lead vehicle mask from the predicted instance masks, as shown in Figure 3-Driving module. To obtain the task-related spatial visual features  $B_t$ , we combine the predicted lead vehicle mask representation  $M_t$  with the lane representation  $G_t$  with an element-wise multiplication. Therefore, each latent vector of  $B_t$  is  $b_{t,j} = g_{t,j} \odot m_{t,j}, j = \{1, 2, \dots, l\}$ .

In addition, we use function  $f_{task}$  to define three main driving tasks that lead to rear-end collisions: *lane-keeping*, *merging-in*, and *braking*. In this function, we consider two criteria: the number of lane changes performed by the ego-vehicle  $c$  and the existence of a traffic signal  $I_{signal}$ . We extract  $c$  and  $I_{signal}$  from VGPNet and MaskTrack-RCNN, respectively.

### 3.3. Attention Module

Drivers pay attention to the task-related regions of the scene to filter out irrelevant information and ultimately make optimal decisions. Drivers do this with a sequence of eye fixations. To learn this process in various driving tasks ending in rear-end collisions, we cast it as a maximum in-

verse reinforcement learning approach. Figure 3 - *attention module* depicts an illustration of the approach.

The state of the agent is defined by the series of perceived information that accumulates over each fixation while performing a task. Therefore, each action of the agent depends on the state at that time and the state changes through each eye fixation  $k$  at time step  $t$ .

**State Representation:** We propose a novel state representation for accumulating task-related visual information through fixations. We create this representation as follows: First, aggregating and smoothing the eye fixations of multiple independent drivers (observers) on a given frame to capture their peripheral vision. Second, formulating the visual systems. The center of attended (fixated) location contains high-resolution visual information. Therefore, the visual inputs outside of the eye fixation location have lower resolution, with the degree of blur which depends on the distance to the eye fixation location. To effectively formulate this system, we use the original frames of the video  $I$  as the high-resolution inputs and a blurred version of the frames to approximate low-resolution input  $L$ . We obtain the blurred frame by applying a Gaussian smoothing with standard deviation  $\sigma = 2 \times n$ , which  $n$  is equal to Euclidean distance between the current fixation point  $p_{k,t}$ , where  $k = 0, \dots, \mathcal{K}$  and the center of bounding box of the target object (e.g., brake lights) at time step  $t$ . Note that the number of fixations  $K$  varies from frame to frame.

Finally, capturing spatial relationship. A driving task along with other task-related objects in a scene can potentially direct visual attention [54]. For example, if the driving task is braking, drivers typically consider the distance between their own vehicle and the lead vehicle. In addition, the road traffic density (i.e. how close the other vehicles are) also determines how fast drivers can reduce the speed. Human fixations also tend to cluster on salient regions that generally correspond to objects and object parts [31, 32]. To approximate this guided movement of fixations, we use the outputs of the visual  $Z_t$  and driving  $B_t$  modules. These visual context information generated by the visual and driving modules can have potential spatial relationship to the driving task. Therefore, they might affect the selection of eye fixations during the driving task. We aggregate the latent vector  $Z_t$  and  $B_t$  by using a position-sensitive ROI average pooling layer to obtain the spatial visual context  $H_t$ .

After applying the mentioned steps, we update the state by replacing the portion of a low-resolution visual feature with the corresponding high-resolution portion obtained at each new fixation location. In this way, we capture the changes in the state representation that occurs following each eye fixation  $k$  at time step  $t$ . We formulate the changes over fixations as follows:  $O_{0,1} = L_{0,1}$ ,  $O_{k+1,t} = E_{k,t} \odot H_t + L_{k,t} \odot O_{k,t}$ , where  $O_{k,t}$  captures the visual information after  $k$  fixations of time step  $t$ .  $E_{k,t}$

is the circular mask generated from the  $k^{th}$  fixation point  $p_k$  of time step  $t$ .  $L_{k,t} = 1 - E_{k,t}$  is extracted spatial visual context from the low-resolution frame for the  $k^{th}$  fixation point  $p_k$  of time step  $t$ .  $H_t$  is the extracted spatial visual context from the high-resolution frame at time step  $t$ . We also consider the changes over each time step  $t$ :  $O_{k,t+1} = E_{k,t+1} \odot H_{t+1} + L_{k,t+1} \odot O_{k,t}$ , where  $O_{k,t+1}$  captures the visual information after  $k$  fixations of time step  $t + 1$ . Then, we use a flattening function  $f_{flatten}$ .

Drivers have different visual attention allocation on the same driving task. To effectively capture this difference, we augment the state by aggregating it with a high-dimensional latent space that encode the driving task  $Q_t$  created from function  $f_{task}$ . We also add an additional fully-connected (FC) layers to encode the current speed of the ego-vehicle in a high-dimensional latent space  $v_t$  as an optional input, which can be excluded from the state representation. Finally, we use additional hidden layers  $f_{state}$  conditioned on the visual context representation, the current speed of the ego-vehicle, and the driving task. The state representation  $S_t$ , which is the set of all states at time step  $t$ , uses bottom-up, top-down and history information through eye fixations.

**Action Space:** We aim to predict the next fixation location of a driver. To cover all types of driving tasks in rear-collisions, we discretize each frame based on the smallest size of the bounding box of the lead vehicle over  $I$ . Action  $a_{k,t}$  represents where the focus of attention can move at fixation  $k$  of time step  $t$ . We apply  $f_{action}$  function which calculates the changes of eye fixation location in 2D-grid space. It defines the following action set: {left, right, up, down, focus-inward, focus-outward, stay}, see Figure 3.  $A_t$  is a set of all actions at time step  $t$ .

**Reward and Policy:** To learn the reward function and policies of visual attention allocation of drivers in rear-end collisions, we use a maximum entropy deep inverse reinforcement learning [49]. Our goal is to select a reward function that encapsulates the intended behavior of attentive drivers. To approximate the reward function associated with taking the action  $a_{k,t}$  in state  $s_{k,t}$ ,  $R(s_{k,t}, a_{k,t}) = \omega^T \phi(s, a)$  which is an inner product between a feature vector  $\phi(s, a)$  extracted from  $s_{k,t}$  and a vector of weights  $\omega$  corresponding to action  $a_{k,t}$ . Due to the large feature space, we use deep architectures in IRL, which increase representational capacity. Therefore, the reward function is  $r \approx \Phi(\phi, \omega, \theta)$ . Note, both the weight vector  $\omega$  and the parameter vector  $\theta$  associated with the network are fine-tuned by jointly training the different driving-tasks categories.

To learn the policies, we maximize the joint posterior distribution of visual attention allocation demonstrations  $\Xi$ , under a given reward structure and of the model parameter,  $\theta$ , across  $I$ . For a single frame and given visual attention allocation sequence  $\xi$  with a length of  $|\tau|$ , which

Data	Method	Merging-in			Lane-keeping			Braking		
		CC $\uparrow$	s-AUC $\uparrow$	KLD $\downarrow$	CC $\uparrow$	s-AUC $\uparrow$	KLD $\downarrow$	CC $\uparrow$	s-AUC $\uparrow$	KLD $\downarrow$
DR(eye)VE [39]	Multi-branch [39]	0.48	0.41	2.80	0.55	0.51	1.87	0.71	0.53	2.20
	HWS [51]	0.51	0.48	2.12	0.75	0.49	1.72	0.74	0.57	1.99
	SAM-ResNet [9]	<b>0.78</b>	0.54	2.01	0.80	0.59	1.80	0.79	0.69	1.89
	SAM-VGG [9]	<b>0.78</b>	0.55	2.05	0.82	0.56	1.84	0.80	0.66	1.81
	TASED-NET [33]	0.68	0.59	1.89	0.73	0.61	1.71	0.70	0.62	1.89
	MEDIRL (ours)	<b>0.78</b>	<b>0.69</b>	<b>0.88</b>	<b>0.89</b>	<b>0.67</b>	<b>0.75</b>	<b>0.85</b>	<b>0.63</b>	<b>0.82</b>
BDD-A [51]	Multi-branch [39]	0.58	0.51	2.08	0.75	0.72	2.0	0.69	0.77	2.04
	HWS [51]	0.53	0.59	1.95	0.67	0.89	1.52	0.69	0.81	1.59
	SAM-ResNet [9]	0.74	0.61	2.00	0.89	0.79	1.83	0.85	0.88	1.89
	SAM-VGG [9]	0.76	0.62	1.79	0.89	0.82	1.64	0.86	0.87	1.85
	TASED-NET [33]	0.73	0.68	1.83	0.81	0.66	1.17	0.87	0.88	1.12
	MEDIRL (ours)	<b>0.82</b>	<b>0.79</b>	<b>0.91</b>	<b>0.94</b>	<b>0.91</b>	<b>0.85</b>	<b>0.93</b>	<b>0.92</b>	<b>0.89</b>
DADA-2000 [14]	Multi-branch [39]	0.44	0.53	3.65	0.69	0.54	2.85	0.67	0.64	2.91
	HWS [51]	0.49	0.59	3.02	0.72	0.53	2.65	0.69	0.77	2.80
	SAM-ResNet [9]	0.65	0.61	2.39	0.78	0.64	2.32	0.75	0.81	2.34
	SAM-VGG [9]	0.68	0.60	2.41	0.76	0.62	2.24	0.75	0.80	2.35
	TASED-NET [33]	0.69	0.66	1.98	0.78	0.69	1.87	0.80	0.81	1.45
	MEDIRL (ours)	<b>0.70</b>	<b>0.68</b>	<b>1.31</b>	<b>0.89</b>	<b>0.71</b>	<b>0.92</b>	<b>0.81</b>	<b>0.88</b>	<b>0.99</b>

Table 2: Comparison of different visual attention allocation models trained on the BDD-A [51] train set using multiple evaluation metrics. We evaluate them with respect to Dr(eye)VE [39], BDD-A [51], and DADA-2000 [14] test sets.

starts from the eye fixation location in a grid cell of the target object without pre-defined goal states, the likelihood is:  $\mathcal{L}_\theta = (1/\Xi) \sum_{\xi^i \in \Xi} \log P(\xi^i, \theta)$ , where  $P(\xi^i, \theta)$  is the probability of the trajectory  $\xi^i$  in demonstration  $\Xi$ .

**Loss Function:** We try to select reward functions with a maximum entropy which minimizes its empirical approximation of the Kullback-Leibler divergence (KLD) between the distributions of generated state-action trajectories of the policies and attentive drivers’ demonstrations.

#### 4. The EyeCar Dataset

Previous works have claimed that in-lab data collection of visual attention is crucial for developing visual attention models [38, 51]. In in-lab settings, participants are free of potential disturbances and can focus on informative areas of the scene. In addition, the in-lab annotation allows us to aggregate the fixation of multiple independent observers to simulate the peripheral vision of human [38]. To that end, herein we construct the EyeCar dataset with in-lab settings. To effectively collect the gaze behavior of drivers for critical situations, we selected videos from the naturalistic driving dataset [12] that included rear-end collisions with high traffic density (see Table 1). During the data collection, we asked participants to ‘task-view’ the collision videos and were free to fix their eyes on their areas of interest. The ‘task-view’ denoted that participants should view the videos under a hypothetical driving task [10].

We select 21 front-view videos that were captured in various traffic, weather, and day light conditions. Each video is 30sec in length and contains typical driving tasks (e.g., lane-keeping, merging-in, and braking) ending to rear-end collisions.

Note that all the conditions were counterbalanced among all the participants. Moreover, EyeCar provides information about the speed and GPS of the ego-vehicle (see Table 1). In addition, each video frame comprises 4.6 vehicles on average, making EyeCar driving scenes more complex than other visual attention datasets. The EyeCar dataset contains 3.5h of gaze behavior (aggregated and raw) from the 20 participants, as well as more than 315,000 rear-end collisions video frames. In EyeCar dataset, we account for the sequence of eye fixations, and thus we emphasize on attention shift to the salient regions in a complex driving scene. EyeCar also provides a rich set of annotations (e.g., scene tagging, object bounding, lane marking, etc.; details in supplementary materials).

#### 5. Experiments

**Datasets.** We use three driving visual attention datasets: DR(eye)VE [39], BDD-A [51], and DADA-2000 [14] as well as EyeCar dataset for evaluation.

To model visual attention allocation related to rear-end collisions, we extract the full stopping events (resembling near-collisions) from DR(eye)VE and BDD-A datasets accompanying rear-end collisions from the DADA-200 dataset. To learn task-sensitive reward functions and policies of attentive drivers, we exclude visual attention allocation sequences that have more than 40 percent of their fixations on the irrelevant objects (e.g., sky, trees, and buildings). This assures us that the attended areas are related to the driving tasks and not their interests as discussed in [16]. The selected sequences show the deviation of the driver’s attention from the common central pattern and denote a linked

Data	Task	Merging-in			Lane-keeping			Braking		
		CC $\uparrow$	s-AUC $\uparrow$	KLD $\downarrow$	CC $\uparrow$	s-AUC $\uparrow$	KLD $\downarrow$	CC $\uparrow$	s-AUC $\uparrow$	KLD $\downarrow$
DR(eye)VE [39]	Multi-branch [39]	0.36	0.37	6.46	0.51	0.49	4.80	0.69	0.49	3.38
	HWS [51]	0.38	0.34	4.38	0.71	0.51	4.44	0.72	0.61	3.30
	SAM-ResNet [9]	0.49	0.48	4.29	0.73	0.55	3.90	0.74	0.66	3.27
	SAM-VGG [9]	0.50	0.47	4.31	0.74	0.53	3.95	0.75	0.64	3.29
	TASED-NET [33]	04.8	0.46	3.95	0.74	0.55	3.81	0.76	0.65	3.23
	MEDIRL (ours)	<b>0.51</b>	<b>0.51</b>	<b>2.32</b>	<b>0.76</b>	<b>0.57</b>	<b>3.11</b>	<b>0.79</b>	<b>0.69</b>	<b>3.07</b>
BDD-A [51]	Multi-branch [39]	0.46	0.48	4.42	0.51	0.61	3.57	0.61	0.64	3.08
	HWS [51]	0.41	0.47	4.36	0.69	0.81	3.55	0.67	0.68	2.86
	SAM-ResNet [9]	0.55	0.48	3.85	0.85	0.72	3.29	0.79	0.74	2.46
	SAM-VGG [9]	0.53	<b>0.49</b>	3.92	0.84	0.70	3.22	0.77	0.70	2.49
	TASED-NET [33]	0.55	<b>0.49</b>	3.78	0.84	0.71	3.12	0.77	0.76	2.47
	MEDIRL (ours)	<b>0.58</b>	<b>0.49</b>	<b>2.81</b>	<b>0.86</b>	<b>0.73</b>	<b>2.43</b>	<b>0.79</b>	<b>0.81</b>	<b>2.30</b>
DADA-2000 [14]	Multi-branch [39]	0.21	0.38	6.46	0.45	0.44	4.67	0.54	0.59	3.12
	HWS [51]	0.31	0.35	6.12	0.51	0.47	4.54	0.67	0.71	3.10
	SAM-ResNet [9]	0.33	0.38	5.28	0.65	0.56	4.42	0.77	0.71	3.07
	SAM-VGG [9]	0.30	0.39	5.35	0.69	0.57	4.31	0.74	0.69	3.10
	TASED-NET [33]	0.32	0.38	4.76	0.68	0.57	3.99	0.73	0.74	3.01
	MEDIRL (ours)	<b>0.41</b>	<b>0.45</b>	<b>3.79</b>	<b>0.73</b>	<b>0.60</b>	<b>2.51</b>	<b>0.75</b>	<b>0.79</b>	<b>2.51</b>

Table 3: Comparison of different visual attention allocation models trained on Dr(eye)VE [39], BDD-A [51], and DADA-2000 [14] train sets. We evaluate these algorithms with respect to EyeCar dataset as the test set.

to task-related actions. Thus, during the policy training, attention module jointly recovers the reward functions and policies used by attentive drivers to predict visual attention allocation.

After applying the exclusion criteria, we were left with 400, 1350, and 534 events in DR(eye)VE, BDD-A, and DADA-200 dataset, respectively. We split each of the datasets into three sets: 70% training, 10% validation, and 20% test, random splits of data, within each driving tasks.

**Training.** We use pre-trained weights in visual and driving modules. The attention module includes four hidden convolutional layers with 52, 34, 20, and 20 ReLU units, respectively; followed by seven softmax units that represent action types (e.g., up, down, etc.). We use batch normalization after ReLU activation. The reward discount factor is set to 0.98. We also set the initial learning rate to  $1.5 \times 10^{-4}$ , and during the first 10 epochs, we linearly increase the learning rate to  $5 \times 10^{-4}$ . After epoch 21, we apply a learning rate decay strategy that multiplies the learning rate by 0.25 every three epochs. Each module has a different structure and learns parameters within its own modular space without affecting other modules. For training, we use Adam optimizer [24]. The total training time of MEDIRL is approximately 1.5 hours on a single NVIDIA Tesla V100 GPU and it takes around 0.08 second to process each frame.

**Evaluation Metrics.** To evaluate the ability of prediction task-related visual attention allocations of drivers in our framework and a number of baselines, we use popular location-based and distribution-based saliency metrics: Kullback-Leibler divergence (KLD), shuffled Area under the ROC curve (s-AUC), and Correlation Coefficient (CC) [6].

We purposefully report s-AUC since it assumes center bias has not been modeled, and penalizes models where it has [6]. We use s-AUC to alleviate the common center-bias of drivers’ visual attention allocation [16].

## 6. Results

To demonstrate the effectiveness of MEDIRL in predicting visual attention allocation of drivers, we compare MEDIRL with five baseline models: Multi-branch [39], HWS [51], SAM-ResNet [9], SAM-VGG [9], TASED-NET [33]. For fair comparisons, we use the implementations with recommended parameters and the saliency maps provided by the authors.

A cross-evaluation of MEDIRL and the selected methods with respect to benchmark datasets are reported in Table 2. The comparison are for three subset of the test sets which involve three driving tasks leading to rear-end collisions. In Table 2, we train the algorithms on the BDD-A train dataset because it is more reflective of visual cues than the other datasets and tested on benchmarks test dataset. As observed from the table, our model outperforms other methods by a significant margin across all evaluation metrics. The cross-evaluation results show that MEDIRL is not strongly tied to a dataset and can adapt to different driving tasks. In addition, we compare the performance of the proposed framework and other methods on the EyeCar dataset (see Table 3). For this set of experiments, we fix the test set (EyeCar) while vary the algorithm and the training datasets, results are reported in Table 3. Overall, the performances of our modular MEDIRL framework in these analyses declares its flexibility and robustness.

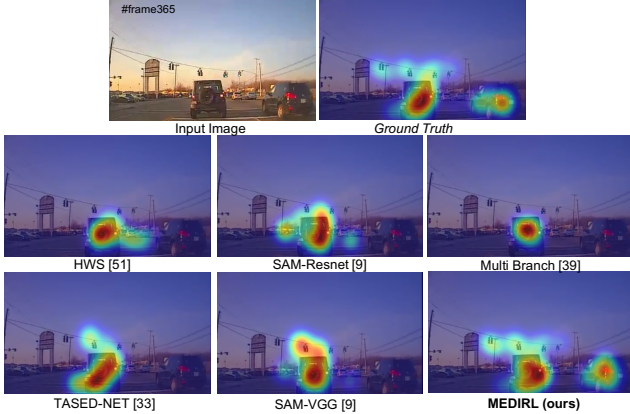


Figure 4: Predicted driver’s visual attention allocation for all models trained on the BDD-A while braking. Although other models partially capture the spatial cues, MEDIRL can learn to completely detect the task-related salient stimuli (e.g., traffic light, brake lights). Redder color indicates the expectation of higher reward for fixating a location.

We also qualitatively compared MEDIRL with baseline models by visualizing driver’s attention predictions in Figure 4. It shows that for nearly every model the attention allocation is entirely toward the center of the video frame, thereby ignoring other cars (i.e., visual spatial cues). In contrast, MEDIRL reliably managed to capture this important information.

To summarize, the experiments show that the proposed MEDIRL framework can effectively learn visual attention policies of attentive drivers. It also correctly reflects typical links between visual spatial cues, which are extracted from bottom-up/top-down mechanisms, and gaze behavior. We observe that our model is indeed able to pay attention on road elements (e.g. traffic signal lights, and the lead vehicle) which are essential for human to drive safely. Therefore, MEDIRL can operate well in complex driving situations with higher visual attention demand.

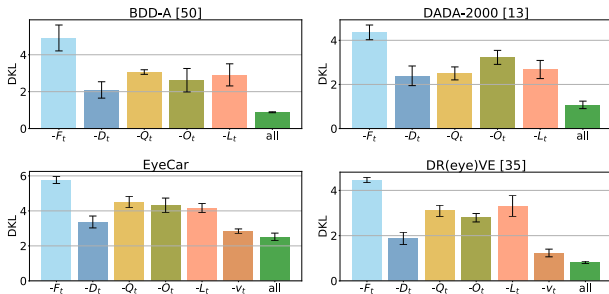


Figure 5: Ablation study on the proposed state representation. We remove one part by masking out or simply removing from the state representation at each time.

	EyeCar			BDD-A [51]		
	CC $\uparrow$	KLD $\downarrow$	$F_\beta$ $\uparrow$	CC $\uparrow$	KLD $\downarrow$	$F_\beta$ $\uparrow$
-visual	0.36	3.55	0.21	0.41	3.51	0.27
-driving	0.69	2.21	0.30	0.60	2.07	0.39
MEDIRL	<b>0.84</b>	<b>0.81</b>	<b>0.61</b>	<b>0.89</b>	<b>0.88</b>	<b>0.78</b>

Table 4: Ablative study of MEDIRL using different combination of modules. The model used here is trained on BDD-A dataset and tested on EyeCar and BDD-A test dataset.

## 6.1. Ablations Studies

**Ablations Studies on State Representation.** Figure 5 shows the ablation study of the full state representation on different test datasets. We can see that the most important feature categories were semantic/instance ( $F_t$ ), followed by types of driving tasks ( $Q_t$ ), the fixation dynamics ( $O_T$ ), and low-resolution visual feature ( $L_t$ ). The depth map features ( $D_t$ ) is also beneficial for the model performance whereas ego-vehicle speed ( $v_t$ ) weakly impacted model performances. The results confirm that incorporation of low and mid-level visual cues, driving-specific visual features, and eye fixations increase the prediction accuracy.

**Ablation Study on Each Module.** We also study the benefits of the visual and driving modules by running ablation experiments (Table 4). We report F-measure score ( $F_\beta$ ), where  $\beta^2$  is set to 1 as suggested [38], as well. Removing the visual module (-visual), which extracts generic visual context features, shows a clear performance drop on EyeCar and BDD-A dataset in terms of all metrics. Without a driving module (-Driving), which extracts driving-specific visual features, all metrics have an obvious decline in both datasets. The results validate the effectiveness of the proposed modular framework that can predict visual attention allocation of drivers since removing one of them degrades the performance.

## 7. Conclusion

We have proposed MEDIRL, a novel modular framework that combines advanced computer vision techniques and inverse reinforcement learning for predicting visual attention of drivers. Our proposed framework learns the task-specific reward functions and the policies of attentive drivers in imminent rear-end collisions. MEDIRL utilizes a combined bottom-up/top-down mechanism to develop a more human-like visual attention allocation model corresponded to drivers’ driving task. We also presented EyeCar, a representative, publicly-available dataset of rear-end collisions driving tasks and richly annotated eye information. These contributions enabled us in establishing a new state-of-the-art in predicting visual attention allocation of drivers on three large-scale benchmarks.



## References

- [1] Pieter Abbeel and Andrew Y Ng. Apprenticeship learning via inverse reinforcement learning. In *Proceedings of the twenty-first international conference on Machine learning*, page 1, 2004. 2
- [2] Peter Anderson, Xiaodong He, Chris Buehler, Damien Teney, Mark Johnson, Stephen Gould, and Lei Zhang. Bottom-up and top-down attention for image captioning and visual question answering. In *Proceedings of the IEEE conference on computer vision and pattern recognition*, pages 6077–6086, 2018. 2
- [3] Ali Borji, Majid Nili Ahmadabadi, Babak Nadjar Araabi, and Mandana Hamidi. Online learning of task-driven object-based visual attention control. *Image and Vision Computing*, 28(7):1130–1145, 2010. 2
- [4] Ali Borji and Laurent Itti. Cat2000: A large scale fixation dataset for boosting saliency research. *arXiv preprint arXiv:1505.03581*, 2015. 3
- [5] Ali Borji, Dicky N Sihite, and Laurent Itti. Probabilistic learning of task-specific visual attention. In *2012 IEEE Conference on Computer Vision and Pattern Recognition*, pages 470–477. IEEE, 2012. 2
- [6] Zoya Bylinskii, Tilke Judd, Aude Oliva, Antonio Torralba, and Frédo Durand. What do different evaluation metrics tell us about saliency models? *IEEE transactions on pattern analysis and machine intelligence*, 41(3):740–757, 2018. 7
- [7] Chenyi Chen, Ari Seff, Alain Kornhauser, and Jianxiang Xiao. Deepdriving: Learning affordance for direct perception in autonomous driving. In *Proceedings of the IEEE International Conference on Computer Vision*, pages 2722–2730, 2015. 1
- [8] Felipe Codevilla, Eder Santana, Antonio M López, and Adrien Gaidon. Exploring the limitations of behavior cloning for autonomous driving. In *Proceedings of the IEEE International Conference on Computer Vision*, pages 9329–9338, 2019. 3
- [9] Marcella Cornia, Lorenzo Baraldi, Giuseppe Serra, and Rita Cucchiara. Predicting human eye fixations via an lstm-based saliency attentive model. *IEEE Transactions on Image Processing*, 27(10):5142–5154, 2018. 2, 6, 7
- [10] Tao Deng, Hongmei Yan, Long Qin, Thuyen Ngo, and BS Manjunath. How do drivers allocate their potential attention? driving fixation prediction via convolutional neural networks. *IEEE Transactions on Intelligent Transportation Systems*, 21(5):2146–2154, 2019. 6, 11
- [11] Tao Deng, Kaifu Yang, Yongjie Li, and Hongmei Yan. Where does the driver look? top-down-based saliency detection in a traffic driving environment. *IEEE Transactions on Intelligent Transportation Systems*, 17(7):2051–2062, 2016. 1
- [12] Thomas A Dingus, Jonathan M Hankey, Jonathan F Antin, Suzanne E Lee, Lisa Eichelberger, Kelly E Stulce, Doug McGraw, Miguel Perez, and Loren Stowe. *Naturalistic driving study: Technical coordination and quality control*. 2015. 6, 11
- [13] Deng-Ping Fan, Wenguan Wang, Ming-Ming Cheng, and Jianbing Shen. Shifting more attention to video salient object detection. In *Proceedings of the IEEE conference on computer vision and pattern recognition*, pages 8554–8564, 2019. 2
- [14] Jianwu Fang, Dingxin Yan, Jiahuan Qiao, Jianru Xue, He Wang, and Sen Li. Dada-2000: Can driving accident be predicted by driver attention analyzed by a benchmark. In *2019 IEEE Intelligent Transportation Systems Conference (ITSC)*, pages 4303–4309. IEEE, 2019. 2, 3, 6, 7
- [15] Keren Fu, Chen Gong, Irene Yu-Hua Gu, and Jie Yang. Normalized cut-based saliency detection by adaptive multi-level region merging. *IEEE Transactions on Image Processing*, 24(12):5671–5683, 2015. 2, 3
- [16] Mingfei Gao, Ashish Tawari, and Sujitha Martin. Goal-oriented object importance estimation in on-road driving videos. In *2019 International Conference on Robotics and Automation (ICRA)*, pages 5509–5515. IEEE, 2019. 2, 6, 7
- [17] Clément Godard, Oisín Mac Aodha, Michael Firman, and Gabriel J Brostow. Digging into self-supervised monocular depth estimation. In *Proceedings of the IEEE international conference on computer vision*, pages 3828–3838, 2019. 4, 13
- [18] Chen Gong, Dacheng Tao, Wei Liu, Stephen J Maybank, Meng Fang, Keren Fu, and Jie Yang. Saliency propagation from simple to difficult. In *Proceedings of the IEEE conference on computer vision and pattern recognition*, pages 2531–2539, 2015. 2, 3
- [19] Max Guangyu Li, Bo Jiang, Zhengping Che, Xuefeng Shi, Mengyao Liu, Yiping Meng, Jieping Ye, and Yan Liu. Dbus: Human driving behavior understanding system. In *Proceedings of the IEEE International Conference on Computer Vision Workshops*, pages 0–0, 2019. 2
- [20] Edwin T Jaynes. Information theory and statistical mechanics. *Physical review*, 106(4):620, 1957. 14
- [21] Fumi Katsuki and Christos Constantinidis. Bottom-up and top-down attention: different processes and overlapping neural systems. *The Neuroscientist*, 20(5):509–521, 2014. 1
- [22] Jinkyu Kim and John Canny. Interpretable learning for self-driving cars by visualizing causal attention. In *Proceedings of the IEEE international conference on computer vision*, pages 2942–2950, 2017. 1, 2
- [23] Jinkyu Kim, Suhong Moon, Anna Rohrbach, Trevor Darrell, and John Canny. Advisable learning for self-driving vehicles by internalizing observation-to-action rules. In *Proceedings of the IEEE/CVF Conference on Computer Vision and Pattern Recognition*, pages 9661–9670, 2020. 2
- [24] Diederik P Kingma and Jimmy Ba. Adam: A method for stochastic optimization. *arXiv preprint arXiv:1412.6980*, 2014. 7
- [25] Mohammadreza Koloushani, Eren Erman Ozguven, Ali Fatemi, and Masoud Tabibi. Mobile mapping system-based methodology to perform automated road safety audits to improve horizontal curve safety on rural roadways. *Computational Research Progress in Applied Science & Engineering (CRPASE)*, 6(4), 2020. 2
- [26] Srinivas SS Kruthiventi, Kumar Ayush, and R Venkatesh Babu. Deepfix: A fully convolutional neural network for predicting human eye fixations. *IEEE Transactions on Image Processing*, 26(9):4446–4456, 2017. 2

- [27] Seokju Lee, Junsik Kim, Jae Shin Yoon, Seunghak Shin, Oleksandr Bailo, Namil Kim, Tae-Hee Lee, Hyun Seok Hong, Seung-Hoon Han, and In So Kweon. Vpynet: Vanishing point guided network for lane and road marking detection and recognition. In *Proceedings of the IEEE international conference on computer vision*, pages 1947–1955, 2017. 4
- [28] Guanbin Li and Yizhou Yu. Visual saliency based on multi-scale deep features. In *Proceedings of the IEEE conference on computer vision and pattern recognition*, pages 5455–5463, 2015. 2, 3
- [29] Ji Hyoun Lim, Yili Liu, and Omer Tsimhoni. Investigation of driver performance with night-vision and pedestrian-detection systems—part 2: Queuing network human performance modeling. *IEEE transactions on intelligent transportation systems*, 11(4):765–772, 2010. 2
- [30] Congcong Liu, Yuying Chen, Lei Tai, Haoyang Ye, Ming Liu, and Bertram E Shi. A gaze model improves autonomous driving. In *Proceedings of the 11th ACM Symposium on Eye Tracking Research & Applications*, pages 1–5, 2019. 2
- [31] Stefan Mathe and Cristian Sminchisescu. Action from still image dataset and inverse optimal control to learn task specific visual scanpaths. In *Advances in neural information processing systems*, pages 1923–1931, 2013. 2, 5
- [32] Stefan Mathe and Cristian Sminchisescu. Actions in the eye: Dynamic gaze datasets and learnt saliency models for visual recognition. *IEEE transactions on pattern analysis and machine intelligence*, 37(7):1408–1424, 2014. 2, 3, 5
- [33] Kyle Min and Jason J Corso. Tased-net: Temporally-aggregating spatial encoder-decoder network for video saliency detection. In *Proceedings of the IEEE International Conference on Computer Vision*, pages 2394–2403, 2019. 2, 6, 7
- [34] Gerhard Neuhold, Tobias Ollmann, Samuel Rota Bulo, and Peter Kontschieder. The mapillary vistas dataset for semantic understanding of street scenes. In *Proceedings of the IEEE International Conference on Computer Vision*, pages 4990–4999, 2017. 3
- [35] Eshed Ohn-Bar, Aditya Prakash, Aseem Behl, Kashyap Chitta, and Andreas Geiger. Learning situational driving. In *Proceedings of the IEEE/CVF Conference on Computer Vision and Pattern Recognition*, pages 11296–11305, 2020. 1
- [36] Erfan Pakdamanian, Lu Feng, and Inki Kim. The effect of whole-body haptic feedback on driver’s perception in negotiating a curve. In *Proceedings of the Human Factors and Ergonomics Society Annual Meeting*, pages 19–23. SAGE Publications Sage CA: Los Angeles, CA, 2018. 1
- [37] Erfan Pakdamanian, Shili Sheng, Sonia Bae, Seongkook Heo, Sarit Kraus, and Lu Feng. Deeptake: Prediction of driver takeover behavior using multimodal data. *arXiv preprint arXiv:2012.15441*, 2020. 1
- [38] Anwesan Pal, Sayan Mondal, and Henrik I Christensen. “looking at the right stuff”-guided semantic-gaze for autonomous driving. In *Proceedings of the IEEE/CVF Conference on Computer Vision and Pattern Recognition*, pages 11883–11892, 2020. 2, 6, 8
- [39] Andrea Palazzi, Davide Abati, Francesco Solera, Rita Cucchiara, et al. Predicting the driver’s focus of attention: the dr (eye) ve project. *IEEE transactions on pattern analysis and machine intelligence*, 41(7):1720–1733, 2018. 1, 2, 3, 6, 7
- [40] Vasili Ramanishka, Yi-Ting Chen, Teruhisa Misu, and Kate Saenko. Toward driving scene understanding: A dataset for learning driver behavior and causal reasoning. In *Proceedings of the IEEE Conference on Computer Vision and Pattern Recognition (CVPR)*, June 2018. 3
- [41] Nathan Sprague and Dana Ballard. Eye movements for reward maximization. In *Advances in neural information processing systems*, pages 1467–1474, 2004. 2
- [42] Benjamin W Tatler, Mary M Hayhoe, Michael F Land, and Dana H Ballard. Eye guidance in natural vision: Reinterpreting saliency. *Journal of vision*, 11(5):5–5, 2011. 2
- [43] Ashish Tawari and Byeongkeun Kang. A computational framework for driver’s visual attention using a fully convolutional architecture. In *2017 IEEE Intelligent Vehicles Symposium (IV)*, pages 887–894. IEEE, 2017. 1
- [44] Sebastian Tschitschek, Ahana Ghosh, Luis Haug, Rati Devidze, and Adish Singla. Learner-aware teaching: Inverse reinforcement learning with preferences and constraints. In *Advances in Neural Information Processing Systems*, pages 4145–4155, 2019. 2
- [45] Jingdong Wang, Ke Sun, Tianheng Cheng, Borui Jiang, Chaorui Deng, Yang Zhao, Dong Liu, Yadong Mu, Mingkui Tan, Xinggang Wang, et al. Deep high-resolution representation learning for visual recognition. *IEEE transactions on pattern analysis and machine intelligence*, 2020. 3
- [46] Wenguan Wang and Jianbing Shen. Deep visual attention prediction. *IEEE Transactions on Image Processing*, 27(5):2368–2378, 2017. 2
- [47] Wenguan Wang, Jianbing Shen, and Ling Shao. Consistent video saliency using local gradient flow optimization and global refinement. *IEEE Transactions on Image Processing*, 24(11):4185–4196, 2015. 2, 3
- [48] Wenguan Wang, Hongmei Song, Shuyang Zhao, Jianbing Shen, Sanyuan Zhao, Steven CH Hoi, and Haibin Ling. Learning unsupervised video object segmentation through visual attention. In *Proceedings of the IEEE conference on computer vision and pattern recognition*, pages 3064–3074, 2019. 2
- [49] Markus Wulfmeier, Peter Ondruska, and Ingmar Posner. Maximum entropy deep inverse reinforcement learning. *arXiv preprint arXiv:1507.04888*, 2015. 2, 5, 14
- [50] Ye Xia, Jinkyu Kim, John Canny, Karl Zipser, Teresa Canas-Bajo, and David Whitney. Periphery-fovea multi-resolution driving model guided by human attention. In *The IEEE Winter Conference on Applications of Computer Vision*, pages 1767–1775, 2020. 1, 2
- [51] Ye Xia, Danqing Zhang, Jinkyu Kim, Ken Nakayama, Karl Zipser, and David Whitney. Predicting driver attention in critical situations. In *Asian conference on computer vision*, pages 658–674. Springer, 2018. 1, 2, 3, 6, 7, 8, 14
- [52] Huazhe Xu, Yang Gao, Fisher Yu, and Trevor Darrell. End-to-end learning of driving models from large-scale video datasets. In *Proceedings of the IEEE conference on computer vision and pattern recognition*, pages 2174–2182, 2017. 1, 3

- [53] Linjie Yang, Yuchen Fan, and Ning Xu. Video instance segmentation. In *Proceedings of the IEEE International Conference on Computer Vision*, pages 5188–5197, 2019. 3, 4
- [54] Zhibo Yang, Lihan Huang, Yupei Chen, Zijun Wei, Seoyoung Ahn, Gregory Zelinsky, Dimitris Samaras, and Minh Hoai. Predicting goal-directed human attention using inverse reinforcement learning. In *Proceedings of the IEEE/CVF Conference on Computer Vision and Pattern Recognition*, pages 193–202, 2020. 1, 2, 3, 5
- [55] Kiwon Yun, Yifan Peng, Dimitris Samaras, Gregory J Zelinsky, and Tamara L Berg. Studying relationships between human gaze, description, and computer vision. In *Proceedings of the IEEE Conference on Computer Vision and Pattern Recognition*, pages 739–746, 2013. 3
- [56] Sara Zahedian, Kaveh Farokhi Sadabadi, and Amir Nohkhan. Localization of autonomous vehicles: Proof of concept for a computer vision approach. In *2019 ITS America Annual Meeting*. ITSWC, 2019. 2
- [57] Gregory J Zelinsky, Yupei Chen, Seoyoung Ahn, Hossein Adeli, Zhibo Yang, Lihan Huang, Dimitrios Samaras, and Minh Hoai. Predicting goal-directed attention control using inverse-reinforcement learning. *arXiv preprint arXiv:2001.11921*, 2020. 2
- [58] Zeyu Zheng, Junhyuk Oh, and Satinder Singh. On learning intrinsic rewards for policy gradient methods. In *Advances in Neural Information Processing Systems*, pages 4644–4654, 2018. 2
- [59] Sheng-hua Zhong, Yan Liu, Feifei Ren, Jinghuan Zhang, and Tongwei Ren. Video saliency detection via dynamic consistent spatio-temporal attention modelling. In *Twenty-seventh AAAI Conference on Artificial Intelligence*, 2013. 2
- [60] Brian D Ziebart, Andrew L Maas, J Andrew Bagnell, and Anind K Dey. Maximum entropy inverse reinforcement learning. In *Aaai*, volume 8, pages 1433–1438. Chicago, IL, USA, 2008. 2, 14

## Appendix

We provide further details about the EyeCar dataset (see Sec. A-1, and implementations (see Sec. A-2. We also provide additional results from experiments and ablation studies (see Sec. A-3). You can find the code and dataset in a zip file.

### A-1. EyeCar

We build EyeCar, a new, diverse dataset of visual driving scenes, driver visual attention together with various tasks. EyeCar covers more realistic driving scenarios in accident-prone situations.

**Participants:** We recruited 20 participants who watched the selected videos. You can find more details of our participants in Table A-1. Note that, each collision video was viewed by all the participants.

**Driving videos:** We selected 21 front-view videos from the naturalistic driving dataset [12] that included rear-end collisions with high traffic density. The videos were captured in

various driving conditions. These conditions contain: traffic conditions (e.g., crowded and not crowded), weather conditions (e.g., rainy and sunny), landscapes (e.g., town and highway), and times of the day (e.g., morning, evening, night). It also contains typical driving tasks (e.g., lane-keeping, merging-in, and braking) ending to rear-end collisions. Each rear-end collision video lasted for 30 seconds, had a resolution of 1280×720 pixels, and had a frame rate of 30 frames per second. All the conditions were counter-balanced among all the participants.

**Study Design:** During the data collection, we asked participants to ‘task-view’ the collision videos and were free to fix their eyes on their areas of interest. The ‘task-view’ denoted that participants should view the videos under a hypothetical driving task [10]. The visual responses and time delay between the onset of the tasks’ stimuli (e.g., brake lights) to perceive it by the participants were captured.

Individuals are eligible to participate in this study if they have normal or corrected to normal vision and have at least one year of driving experience. After enrolling in the program, individuals are asked to fill out initial questions consisting of their age, driving experience, gender, whether they have experience with the semi-autonomous vehicle or not, and if they have been involved in any car accidents or not (see Table A-1). The study had two sessions, and each lasts for 7±2 minutes. To decrease the chance of drivers fatigue and disengagement, participants watched the first 10 videos in the first session, and then after 15 minutes gap, they watched the other 11 videos in the second session (the whole study takes less than half an hour). The experiment received ethical approval from the University’s Institutional Review Board.

**Apparatus:** We conducted this study in an experiment booth with controlled lighting. The experiment was designed to maximize the accuracy of the eye tracker to be used as the ground truth for the evaluation of the estimated driver attention allocation. The driving scenes were displayed on a 20-inch monitor with a pixel resolution of 2560 by 1440 and. Participants were seated approximately 60 cm away from the screen. The head was stabilized with a chin and forehead rest. A steering wheel is placed in front of the participants who were asked to view the videos by assuming that they were driving a car. To control the lighting and minimize possible shadows, a Litepanels LED-daylight was used.

Eye movements were recorded using the screen-mounted Tobii X3-120 system with a sampling rate of 120 Hz. The eye-tracker was mounted under the screen of the monitor placed in front of the participants. Due to the sensitivity of the eye tracker, the vertical placement of the screen was adjusted such that the center of the screen was at eye-level for each participant. The system had to be calibrated for each participant using the Tobii Pro Studio animating nine

Gender	Age	Driving Experience	Semi-autonomous vehicle	Accident
75%(male)	27.31 ( $\pm$ 4.81)	9.71( $\pm$ 5.8)	25%	1%

Table A-1: Detailed information about individuals who participate in the study.

Dataset	Videos	Accidents	Events	Gaze providers	Duration(hrs)	Number of Frames	Annotation type	Gaze pattern (per frame)	Fixations
EyeCar	21	21	rear-end collisions	20	3.5	315K	spatial and temporal	raw and average	1,823,159

Table A-2: The EyeCar dataset detailed information.

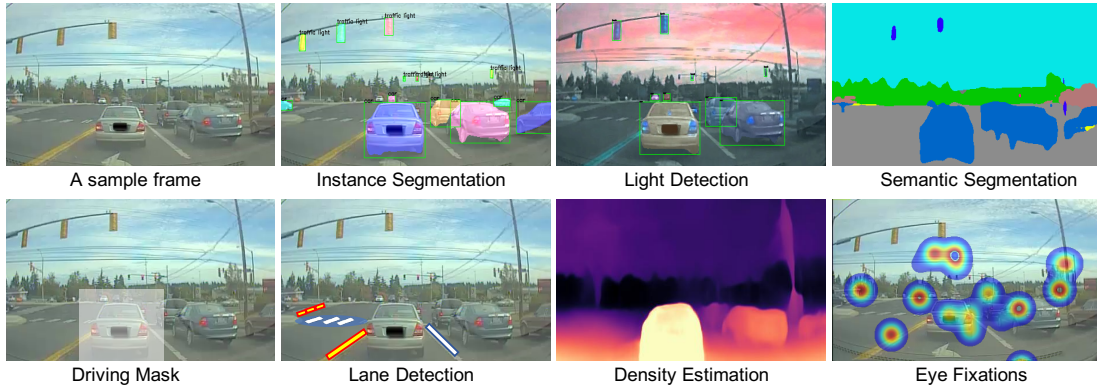


Figure A-1: Overview of our dataset. The dataset also comes with a rich set of annotations: object bounding, lane marking, full-frame semantic and instance segmentation.

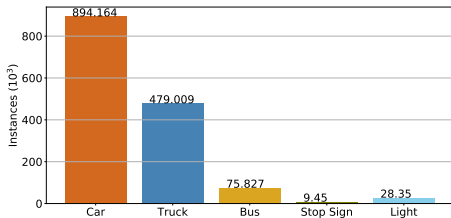


Figure A-2: The distribution of typical instances categories involved in an accident over all frames of the EyeCar videos.

calibration points. Calibration accuracy was then recorded to be within 0.6 degrees of visual angle for both axes of all participants.

### A-1.1. Data Preprocessing:

**Driving videos:** EyeCar comes with a rich set of annotations: object bounding, lane marking, full-frame semantic, and instance segmentation (see Figure A-1). You also can see the number of typical instances involved in an accident over all frames of videos in Figure A-2.

**Eye information:** We employ iMotion to extract the eyes' features such as; pupil size, gaze location, fixation duration, the sequence of fixation, and the start and end time of the fixation points. The abnormal or missing values of these features can lead us to the wrong conclusion, therefore pre-processing of the raw data is necessary for identifying such

values and replacing them with linearly interpolated values, outlier treatment, statistical analysis, and data quality (e.g., calibration, exclusion of trials and participants due to poor recording, track loss).

To clean the data, we first extract the missing values of the eyes' features. We employ linear interpolation if the percentage of the missing values is less than 20%. Then, we calculated the abnormal values of features to detect the outliers. We calculated the mean ( $\mu_{feature}$ ) and the standard deviation ( $\sigma_{features}$ ) of each feature (zero values are excluded from our calculation) for each participant. Then, we set the low and high threshold as follows:

$$\begin{aligned} \text{low threshold} &= \mu_{feature} - 3 \times \sigma_{feature} \\ \text{high threshold} &= \mu_{feature} + 3 \times \sigma_{feature} \end{aligned}$$

Abnormal values are those that their values are less than low threshold and more than a high threshold. In addition to the exclusion criteria described in the main text, we also excluded the sequences with more than 40% abnormal values for eye fixations. In this way, we decreased the chance of drivers fatigue and disengagement. We have about 0.005% of sequences with this conditions.

**EyeCar dataset:** After implemented all exclusion criteria, we selected 416 variable-length sequences. EyeCar includes more than 315,000, rear-end collisions video frames. In addition, each video frame comprises 4.6 vehicles on average, making EyeCar driving scenes more complex than other visual attention datasets. GPS recordings in our

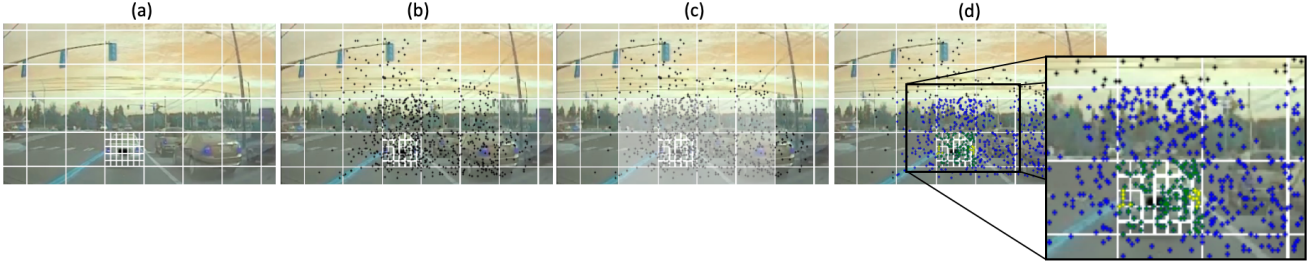


Figure A-3: Illustration of a discretize frame along with gaze location points of all drivers in the EyeCar dataset. Drivers allocate their attention to the driving task-related salient regions of the driving scene. The points show the gaze location of drivers. The black points are out of the task-related regions. The blue points are in the driving mask (the gray area in the frame). The green points are in the lead vehicle bounding box, and the yellow points are in the area of the target object (i.e., braking lights).

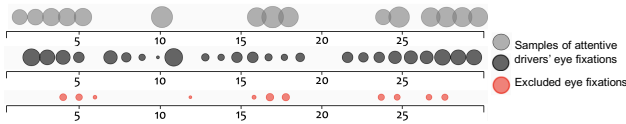


Figure A-4: A sample of attentive drivers' average eye fixation sequence for a given front-view video as well as the excluded sequence. Note that the sizes of the circles are corresponding to the duration of the average eye fixation over the last 30 frames before a collision.

dataset show the human driver action given the visual input and the driving trajectories. The proportion of high ( $65 \leq v$ ), normal ( $35 \leq v \leq 65$ ), and low ( $35 \geq v$ )-speed categories are 38%, 39%, and 23%, respectively.

A total of 1,823,159 fixations were extracted from the eye position data, over the 20 subjects. The EyeCar dataset contains 3.5h of gaze behavior from the 20 participants. We also provide a raw fixation map of multiple observers as well as an average fixation map of them. You can see the detailed information of EyeCar in Table A-2. The fixation maps highlight the direction of human drivers' gaze to a salient object when making driving decisions in rear-end collisions. EyeCar comes with information of eye fixations (fixation maps and duration, start and end time, positions, and pupil size), distance to the target object (e.g., brake lights), and the location of the target objects and their temporal occurrence interval.

## A-2. Implementation

Given a set of driving video's frames,  $I = \{I_t\}_{t=1}^T$ , we resize each of them to  $144 \times 256 \times 3$ , where  $T$  is the number of frames. Then we normalize each frame by subtracting the global mean from the raw pixels and dividing by the global standard deviation.

**Depth Estimation:** Recognizing the relative distance to the other traffic participants (e.g., the lead vehicle) is crucial for making optimal driving decisions. Therefore, we



Figure A-5: Examples of MEDIRL generated visual attention allocations on EyeCar dataset. An attentive driver eye fixation sequences are colored in green, and the model generated are in blue. You can see that MEDIRL mainly focused on driving tasks related to rear-end collisions.

use a supervised monocular depth estimation model, Monodepth2 [17], to amplify nearby regions (e.g., distance to a target object) of a driving scene. The predicted dense depth map  $D_t$  at each time step  $t$  is combined with the visual feature  $F_t$  by the following formula:

$$F_t \oplus D_t = F_t \odot \lambda * D_t + F_t,$$

where  $\lambda = 1.2$ . This value of *lambda* parameter helped us to focus on the lead vehicle more than other surrounding vehicles during rear-end collisions. Note that the above equation is equivalent to the main paper's equation which is written in a recurrent form.

**State Representation:** In our proposed state representation, we try to formulate the visual system mechanism by considering the high-resolution visual information in eye fixation location and low-resolution visual information outside of the eye fixation location. To approximate low-resolution input  $L$ , we apply a Gaussian smoothing with standard deviation  $\sigma = 2 * n$ , which  $n$  is equal to Euclidean distance between the current fixation point  $p_{k,t}$ , and the center of bounding box of the target object (e.g., brake lights) at time step  $t$ . We selected 2 as the degree of blur's parameter, experimentally. We also tried 0.5, 1, and 1.5 but we got a better formation by 2. Note that the number of fixations  $K$  varies from frame to frame.

Line		EyeCar			BDD-A [51]		
		CC $\uparrow$	KLD $\downarrow$	$F_\beta \uparrow$	CC $\uparrow$	KLD $\downarrow$	$F_\beta \uparrow$
1	MEDIRL:( $F$ ) + ( $E$ ) + attention	0.25	3.81	0.17	0.36	3.88	0.22
2	MEDIRL:( $F + D$ ) + ( $E$ ) + attention	0.30	3.62	0.19	0.38	3.77	0.27
3	MEDIRL:( $F + D$ ) + ( $Q$ ) + ( $E$ ) + attention	0.34	3.61	0.20	0.37	3.78	0.29
4	MEDIRL:( $F + D$ ) + ( $Q$ ) + ( $L$ ) + ( $E$ ) + attention	0.49	3.02	0.26	0.56	2.87	0.33
5	MEDIRL:( $F + D$ ) + ( $Q$ ) + ( $L$ ) + ( $O$ ) + ( $E$ ) + attention	0.69	2.21	0.30	0.60	2.07	0.39
6	MEDIRL:( $F$ ) + ( $G + M$ ) + ( $E$ ) + attention	0.30	3.43	0.23	0.29	3.47	0.32
7	MEDIRL:( $F + D$ ) + ( $G + M$ ) + ( $E$ ) + attention	0.33	3.13	0.26	0.35	3.07	0.34
8	MEDIRL:( $F + D$ ) + ( $Q$ ) + ( $G + M$ ) + ( $E$ ) + attention	0.49	2.51	0.30	0.51	2.17	0.39
9	MEDIRL:( $M + G$ ) + ( $E$ ) + attention	0.36	3.55	0.21	0.41	3.51	0.27
10	MEDIRL:( $F + D$ ) + ( $Q$ ) + ( $O$ ) + ( $L$ ) + ( $G$ ) + ( $E$ ) + attention	0.71	1.41	0.42	0.67	1.18	0.59
11	MEDIRL:( $F + D$ ) + ( $Q$ ) + ( $O$ ) + ( $L$ ) + ( $M$ ) + ( $E$ ) + attention	0.76	1.11	0.49	0.73	1.07	0.66
12	MEDIRL:( $F + D$ ) + ( $Q$ ) + ( $O$ ) + ( $L$ ) + ( $G + M$ ) + ( $E$ ) + attention	0.80	0.78	0.60	0.87	0.87	0.75
13	<b>MEDIRL:(<math>F + D</math>) + (<math>Q</math>) + (<math>O</math>) + (<math>L</math>) + (<math>G + M</math>) + (<math>v</math>) + (<math>E</math>) + attention</b>	<b>0.84</b>	<b>0.81</b>	<b>0.61</b>	<b>0.89</b>	<b>0.88</b>	<b>0.78</b>

Table A-3: An ablative study of MEDIRL using different combination of modules. The model used here is trained on BDD-A dataset and tested on EyeCar and BDD-A [51] test set. We mask out one part by setting the map(s) to zeros at each time.

**Action Space:** We aim to predict the next eye fixation of drivers. Therefore, we need to predict the pixel location where the driver is looking in the driving scene during accident-prone situations. We discretize each frame based on the smallest size of the bounding box of the lead vehicle in a given video (see Figure A-3. The maximum approximation error due to this discretization procedure is 1.27 degrees, visual angle. Action  $a_{k,t}$  represents where the focus of attention can move at fixation  $k$  of time step  $t$ . We apply  $f_{action}$  function which calculates the changes of eye fixation location in 2D-grid space:  $f_{action} = (\Delta_x, \Delta_y)$ . Therefore, we summarized the action set as follows: {left, right, up, down, focus-inward, focus-outward, stay} with three degrees of freedom (vertical, horizontal, diagonal).

At each step, the policy chooses one of the patches (grid cell), and the central location of the selected patch in the original image coordinates is used for the eye fixation. We also excluded the patches that have no visit or less than 5 visits for computational efficiency. It should be noted that we did not pre-defined the radius of the direction for the agent. Therefore, the agent has the freedom to pick any patch among the created ones.

**Driving task:** To consider the driving tasks that ends to rear-end collisions, we consider two following criteria in the function  $f_{task}$ : the number of lane changes performed by the ego-vehicle  $c$  and the existence of a traffic signal  $I_{signal}$  over  $I$ . We extract  $c$  and  $I_{signal}$  from VGPNet and MaskTrack-RCNN, respectively. Therefore, we define the driving task as follows:

$$\text{driving task} = \begin{cases} \text{lane-keeping,} & \text{if } c = 0, \text{ and } I_{signal} = 0 \\ \text{braking,} & \text{if } c = 0, \text{ and } I_{signal} = 1 \\ \text{merging-in,} & \text{if } c = 1, \text{ and } I_{signal} = 0 \end{cases}$$

We embed the task in our framework by one-hot encoding maps which spatially repeat the one-hot vector. There-

fore, we concatenate the task embedding with other features in our proposed state representation to have a task-dependent bias term for every convolutional layer.

**Visual attention allocations:** The eye fixation location is generated from the probability map that MEDIRL has produced. We also applied Inhibition-of-Return to decrease the likelihood that a previously inspected (possibly salient) region in the scene will be re-inspected, thereby encouraging visual attention toward the next salient region in a driving scene. Therefore, MEDIRL generates a new spatial probability map at every step.

**Maximum Entropy:** To learn the policies, we maximize the joint posterior distribution of visual attention allocation demonstrations  $\Xi$ , under a given reward structure and of the model parameter,  $\theta$ , across  $I$ . For a single frame and given visual attention allocation sequence  $\xi$  with a length of  $|\tau|$ , which starts from the eye fixation location in a grid cell of the target object without pre-defined goal states, the likelihood is:  $\mathcal{L}_\theta = (1/|\Xi|) \sum_{\xi^i \in \Xi} \log P(\xi^i, \theta)$ , where  $P(\xi^i, \theta)$  is the probability of the trajectory  $\xi^i$  in demonstration  $\Xi$ . In each iteration  $j$  of maximum entropy deep inverse reinforcement learning algorithm, we first evaluate the reward value based on the state features and the current reward network parameters  $\theta_j$ . Then, we determine the current policy,  $\pi_j$ , based on the current approximation of reward,  $R_j$  and transition matrix (i.e., the outcome state-space of a taken action),  $\mathcal{T}$ . Therefore, we can benefit from the maximum entropy paradigm, which enables the model to handle sub-optimal behavior as well as stochastic behavior of experts, by operating on the distribution over possible trajectories [60, 49].

Principle of Maximum Entropy [20] demonstrates that the best distribution over current information is one with the largest entropy. Maximum Entropy also prevents issues

with label bias which means portions of state space with many branches will each be biased to be less likely, and while areas with fewer branches will have higher probabilities (locally greedy). Maximum Entropy gives all paths equal probability due to equal reward and uses a probabilistic approach that maximizes the entropy of the actions, allowing a principled way to handle noise, and it prevents label bias. It also provides an efficient algorithm to compute empirical feature count, leading to a state of the art performance at the time. This process maximized total reward, even over the short period of time ( $0.6 \pm 0.2$  seconds) that our attentive drivers detect the target objects (brake light) in rear-end collisions.

### A-3. Ablation Studies

We study the benefits of each component of MEDIRL by running ablation experiments (see Table A-3) with the trained model on the BDD-A dataset and tested on EyeCar and BDD-A test dataset. We employed our visual and driving modules to have a rich state representation for our proposed MEDIRL framework. To understand the contribution of each component, we removed the maps of each group one at a time and compared the corresponding performance of the model.

A front-view video of an accident-prone situation paired with eye fixation is our input. Utilizing these two features as a baseline (Line 1). Line 2 shows the benefit of encoding the relative distance to the other traffic participants (e.g., the lead vehicle) (Sec. 3.1). After adding the driving task, the performance further improves (Line 3). Line 4 shows the benefits brought by low-resolution, and we find the update of the visual systems in the visual attention allocations of drivers (Line 5) considerably improves on the performance, demonstrating the advantages of visual systems in a proposed state representation on detecting task-related salient regions. Line 6, 7, and 8 show the benefit of the visual systems update in eye fixation and the encoding of the driving task. The task-related features without the visual features are not very beneficial for the visual attention allocation performance (Line 9). Line 10, 11, 12 demonstrate that driving-specific visual features are beneficial for task-related visual attention allocation. We find the ego-vehicle speed slightly improves on visual attention allocation of drivers but not in terms of KLD metrics (Line 13).